STRUCTURE OF A DAYTIME CONVECTIVE BOUNDARY LAYER REVEALED BY A VIRTUAL RADAR BASED ON LARGE EDDY SIMULATION

D. E. Scipión[1,2,*], R. D. Palmer[2], E. Fedorovich[2], P. B. Chilson[2], A. M. Botnick[2]

[1] School of Electrical and Computer Engineering, University of Oklahoma, Norman, Oklahoma, USA
[2] School of Meteorology, University of Oklahoma, Norman, Oklahoma, USA

Abstract

The daytime atmospheric convective boundary layer (CBL) is characterized by strong turbulence that is primarily caused by buoyancy forced from the heated underlying surface. The present study considers a combination of radar and large eddy simulation (LES) techniques to characterize the CBL. Data representative of the daytime CBL with wind shear have been generated by LES, and used in the virtual boundary layer radar (BLR) with multiple vertical and off-vertical beams. A multiple radar experiment (MRE) was conducted using five virtual BLRs located equidistant within the LES, and pointing into the same resolution volumes at many altitudes. Three-dimensional wind fields were retrieved from the radar and compared with the LES output. Finally, the three-dimensional wind fields obtained from the MRE are used to estimate the turbulent kinetic energy and the turbulent kinematic momentum fluxes. These data are then compared with LES statistics for a time average vertical profile at the center of the domain.

1. INTRODUCTION

Turbulence in the daytime atmospheric convective boundary layer (CBL) is primarily forced by heating of the surface, radiational cooling from clouds at the CBL top, or by both mechanisms. The CBL is considered clear when no clouds are present [Holtslag and Duynkerke, 1998], as in this study. In this case, the main forcing mechanism in the CBL is heating of the surface.

Turbulent convective motions in the CBL transport heat upward in the form of convective plumes or thermals. These rising motions and associated downdrafts effectively mix momentum and potential temperature fields in the middle portion of the CBL [Zilitinkevich, 1991]. The resulting mixed layer is typically the thickest sublayer within the CBL. The CBL is topped by the entrainment zone, with relatively large vertical gradients of averaged (in time or over horizontal planes) meteorological fields. The entrainment zone is often called the interfacial or capping inversion layer, as it is collocated with the region of maximum gradients in the potential temperature profile.

A widely used instrument for the study and monitoring of the lower atmosphere is the boundary layer radar (BLR). The term BLR is generally applied to a class of pulsed Doppler radar that transmits radio waves vertically, or nearly vertically, and receives Bragg backscattered signals from refractive index fluctuations of the optically clear atmosphere. The operating frequency of this type of radar is typically near 1 GHz. Therefore, the Bragg scale is such that BLRs are sensitive to turbulent structures, which have a spatial scales near 15 cm. Enhanced refractive index variations are often associated with the entrainment zone just above the CBL, which can be detected by clear-air radar. There have been many studies in which BLRs are used to estimate the height of the atmospheric boundary layer (ABL) and thickness of the entrainment layer [e.g., Angevine et al., 1994; Angevine, 1999; Cohn and Angevine, 2000; Grimsdell and Angevine, 2002]. Profiles of the wind vector directly above the instrument are obtained using the Doppler beam swinging (DBS) method [Balsley and Gage, 1982]. BLRs are also sensitive to Rayleigh scatter from hydrometeors and are used to study clouds and precipitation [Gage et al., 1994; Ecklund et al., 1995]. Thus, the BLR can be used to study the boundary layer under a wide variety of meteorological conditions, and has been proven invaluable for such investigations [e.g., Rogers et al., 1993; Angevine et al., 1994; Wilczak et al., 1996; Dabberdt et al., 2004].

Complementary to field observations of the CBL by *in-situ* and remote sensing measurement methods, numerical simulation approaches – specifically, the large eddy simulation (LES) technique – are widely employed to study physical processes in the atmospheric CBL.

The LES method is based on the numerical integration of filtered equations of flow dynamics and thermodynamics that resolve most of the energy-containing scales of turbulent transport. Any motions that are not

* *Corresponding author address:* Danny E. Scipión, University of Oklahoma, School of Meteorology, 120 David L. Boren Blvd., Rm 5900, Norman, OK 73072-7307; e-mail: dscipion@ou.edu

resolvable are assumed to carry only a small fraction of the total energy of the flow, and are parameterized with a subgrid (or subfilter) closure scheme. In the LES of the atmospheric CBL, the environmental parameters such as surface heating, stratification, and shear can be precisely controlled.

In addition to adopting LES and radar methodologies as is conventionally done, in the present investigation, these two approaches have been synthesized through the development and implementation of an enhanced radar simulator based on the work of Muschinski et al. [1999]. High resolution three-dimensional wind and thermodynamic fields representing a clear CBL are generated using LES. These data are then probed using a virtual ultra high frequency (UHF) BLR, similar to those conventionally used in numerous atmospheric studies and field campaigns.

As mentioned, the time-series data for the virtual BLR are generated following the approach developed in Muschinski et al. [1999], which are compiled by summing the contribution from each point within the radar resolution volume. This is determined by the radar pulse and beam width. The virtual BLR output data are then employed to estimate CBL characteristics, which are compared to the "ground-truth" (reference) LES data. Comparison between the components of the velocity vector from the BLR and LES, as well as, turbulent kinetic energy and turbulent kinematic momentum fluxes computed over an hour of simulation time, are presented in this work.

2. ESTIMATION OF THE STRUCTURE FUNCTION PARAMETER OF REFRACTIVITY FROM THE LES

The LES code employed in the present study has been developed along the lines described in Nieuwstadt [1990]; Fedorovich et al. [2001, 2004]. With respect to many of its features, the code was specifically designed to simulate CBL-type flows characterized by the presence of large-scale turbulent structures transporting the dominant portion of the kinetic and thermal energy of the flow. Fields of atmospheric parameters generated by LES are used as input fields for the BLR simulator.

The simulation run for the present study has been performed in a rectangular domain composed of 10 m grid cells. The domain size is $X\times Y\times Z$ = 5120×5120×2000 m^3. Correspondingly, there are 512×512×200 grid points. The time discretization is 1 s. The following external parameters were assigned for the run; the free-atmosphere horizontal wind was set to 5 m s^{-1} in the x direction and 0 m s^{-1} in the y direction; the free-atmosphere potential temperature gradient was 0.004 K m^{-1}; the surface kinematic heat flux, surface kinematic moisture flux, and the surface roughness length were 0.2 K m s^{-1}, 10^{-4} m s^{-1}, and 0.01 m, respectively.

A subset of the LES output was used for the radar simulator. The radar sub-domain size was 1060 m $\leq x \leq$ 4060 m, 1060 m $\leq y \leq$ 4060 m, and 0 m $\leq z \leq$ 1600 m. The output included resolved (in the LES sense) three-dimensional fields of potential temperature Θ, specific humidity q, flow velocity components u, v and w, and subgrid turbulence kinetic energy E, as presented in Fig. 1, and summarized in Table 1. See Conzemius and Fedorovich [2006] for additional information about the numerical setup.

Table 1: Description of the LES sub-domain used by the radar simulator

Property	Specification
Number of grid points	300×300×160
Spatial resolution	10 m
Time step	1 s
Dim. of the sub-domain	3000×3000×1600 m^3
Variables	u, v, w, E, q, Θ

According to the radar equation, the backscattered signal power from a collection of distributed targets is directly proportional to the radar reflectivity η. The value of η represents the cumulative effect of the radar cross sections for the individual targets. For the case of scatter resulting from turbulent variations in the refractive index (clear-air scatter), the echo power is also related to the radar reflectivity; however, η is now given by the well established theoretical relationship

$$\eta = 0.379 C_n^2 \lambda^{-1/3}, \tag{1}$$

where C_n^2 is the structure function parameter of the refractive index, and λ is the radar wavelength [Tatarskii, 1961; Ottersten, 1969]. It is assumed that the turbulence is isotropic and in the inertial subrange. Further, the radar resolution volume is assumed to be uniformly filled with turbulence.

The structure function parameter of refractivity, C_n^2, is by definition derived from the refractive index field using

$$C_n^2 = \frac{\left\langle [n(r+\delta) - n(r)]^2 \right\rangle_r}{|\delta|^{2/3}}, \tag{2}$$

where n is the refractive index and $< \cdot >_r$, as mentioned in Muschinski et al. [1999]. This denotes the spa-

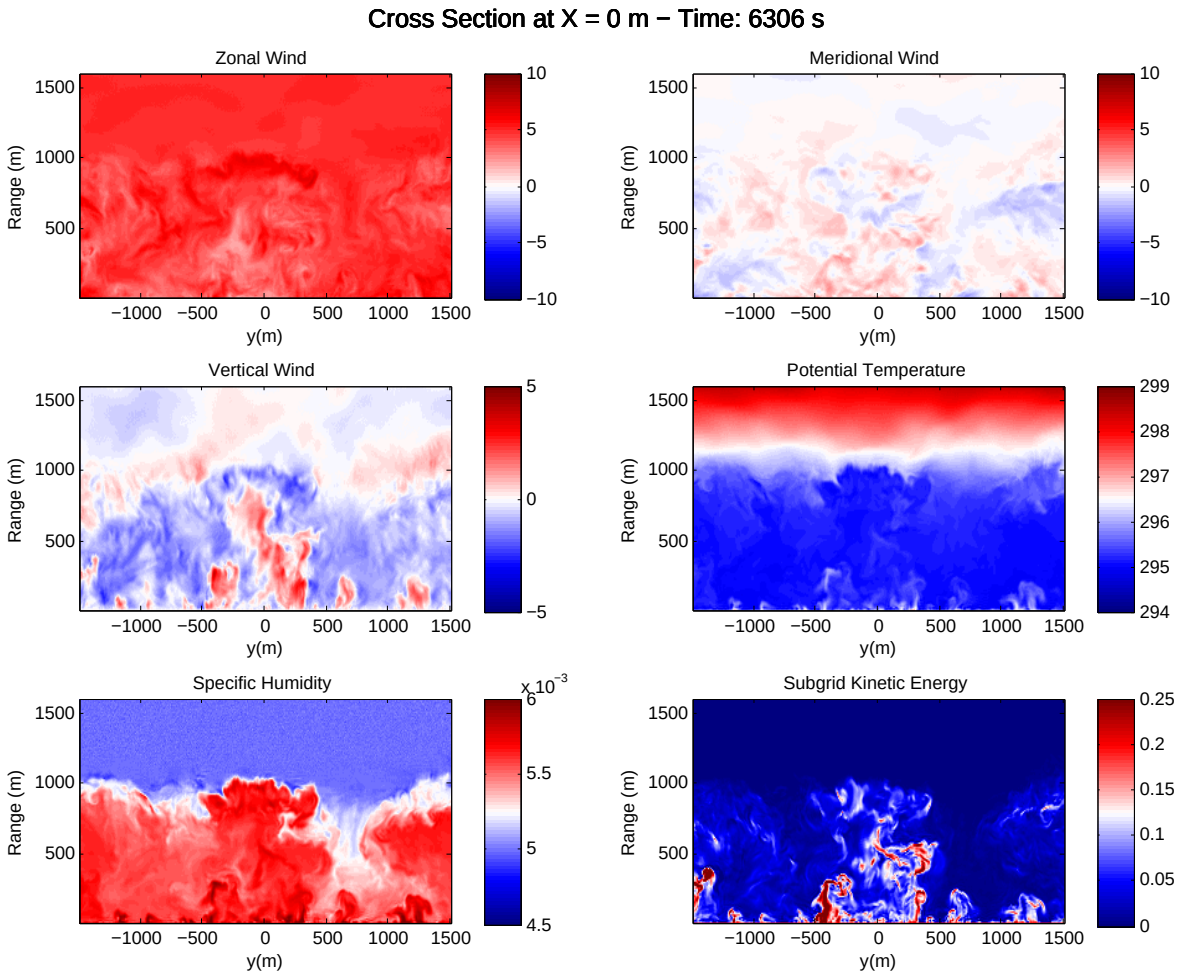

Figure 1: Examples of LES output fields in the sub-domain of the radar simulator. Top-left: zonal wind. Top-right: meridional wind. Middle-left: vertical velocity. Middle-right: potential temperature. Bottom-left: specific humidity. Bottom-right: subgrid kinetic energy. All data presented refer to the same single realization in time (one LES time step).

tial average over a volume within which the n irregularities are assumed to be statistically isotropic and homogeneous. Here, r represents the position vector, and δ denotes the spatial separation.

The refractive index is related to the refractivity, N, through $n = 1 + N \times 10^{-6}$. If we assume that the background atmospheric pressure profile is hydrostatic, then the refractivity is found directly from the simulation output parameters through the following equations [Bean and Dutton, 1966; Holton, 2004]:

$$N = \frac{77.6}{T}\left(P + 4811\frac{e}{T}\right), \quad (3)$$

$$\mathrm{d}\ln P = -\frac{g}{RT}\mathrm{d}z, \quad (4)$$

$$T = \Theta\left(\frac{P}{P_0}\right)^{0.286}, \quad (5)$$

$$e = \frac{qP}{0.622 + q}, \quad (6)$$

where P is the atmospheric pressure (hPa), $e(q, T)$ is the partial pressure of water vapor (hPa), g is the gravitational acceleration (9.81 m s^{-1}), R is the gas constant for dry air (287 J kg $^{-1}$ K $^{-1}$), and T is the absolute temperature (K).

To calculate C_n^2 within each grid cell of the LES domain, Eq. 2 was applied along a line (beam) connecting the position of the virtual radar and the center of the grid cell where C_n^2 needed to be estimated (Fig. 2: left). Then, the refractive index n was calculated in the center of the grid cell at a level z with respect to the ground and at two levels displaced from z in height by an increment Δz (Fig. 2: right). That is, the points at z, $z - \Delta z$, and $z + \Delta z$ are considered. A bilinear interpolation was then applied in order to obtain an estimate of n between the closest 4 points on the upper and lower planes, thereby calculating values of n along the beam:

$$\begin{aligned} n_{xy} &= (1-dx)(1-dy)n_{x0y0} + \\ &\quad (dx)(1-dy)n_{x1y0} + (1-dx)(dy)n_{x0y1} + \\ &\quad (dx)(dy)n_{x1y1}, \quad (7) \\ dx &= \frac{x - x_0}{x_1 - x_0}, \quad dy = \frac{y - y_0}{y_1 - y_0}, \end{aligned}$$

where n_{xy} represents the refractive index n at point (x, y), which does not match any of the grid points, and n_{xiyj} denotes refractive index values at x_i,y_j; $i, j = 0, 1$.

Since the radar is sensitive to variations in the refractive index on the order of the Bragg scale ($\lambda/2$ ~16 cm for a frequency of 915 MHz), which is much smaller than the LES grid cell size (10 m), one may assume the simulated turbulence to be approximately isotropic on the scales sensed by the radar; however, the estimation of C_n^2 needs to be rescaled by $\lambda/2$ to accurately represents the Bragg scale. This modification along with the average over two consecutive layers constitute a significant refinement from the work of Muschinski et al. [1999]:

$$C_n^2(x, y, z, t) = \frac{1}{2}\left[\frac{\left(\frac{n_1 - n}{\delta} \cdot \frac{\lambda}{2}\right)^2}{\left(\frac{\lambda}{2}\right)^{2/3}} + \frac{\left(\frac{n - n_2}{\delta} \cdot \frac{\lambda}{2}\right)^2}{\left(\frac{\lambda}{2}\right)^{2/3}}\right], \quad (8)$$

where n_1, n, and n_2 represents the refractive index at levels $z + \Delta z$, z, and $z - \Delta z$ respectively, as depicted in Fig. 2: right, and λ is the wavelength of the radar. An example vertical profile of the specific humidity q, from the LES output together with the corresponding calculated profiles of refractivity N, and the horizontal averaged structure function parameter of refractivity, C_n^2 are presented in Fig. 3 for a single realization in time.

3. RADAR SIMULATOR

Various approaches can be found in the literature to be used in generating time-seres data for radar simulations. One that was studied by Sheppard and Larsen [1992]; Holdsworth and Reid [1995]; Yu [2000]; Cheong et al. [2004] consists of creating a *sampling domain* populated with scattering points. These points move within the domain according to the field of instantaneous wind vector. Another method considers the grid cells of the model as a scattering center, and the phase of the radar signal from the scattering center is modulated by the local instantaneous velocity field [Muschinski et al., 1999]. Therefore, by varying the phase, without actually moving the scatterer, the expected Doppler velocity can be generated. Some implementation advantages exist with such a method, especially related to scatterer position update.

The radar simulator for this study was developed following the Eulerian frame approach of Muschinski et al. [1999]. The signal amplitude in the simulator after time τ is proportional to C_n^2 and inversely proportional to r_0^2, which is the range of the center of the sampling volume. The phase difference is proportional to the velocity vec-

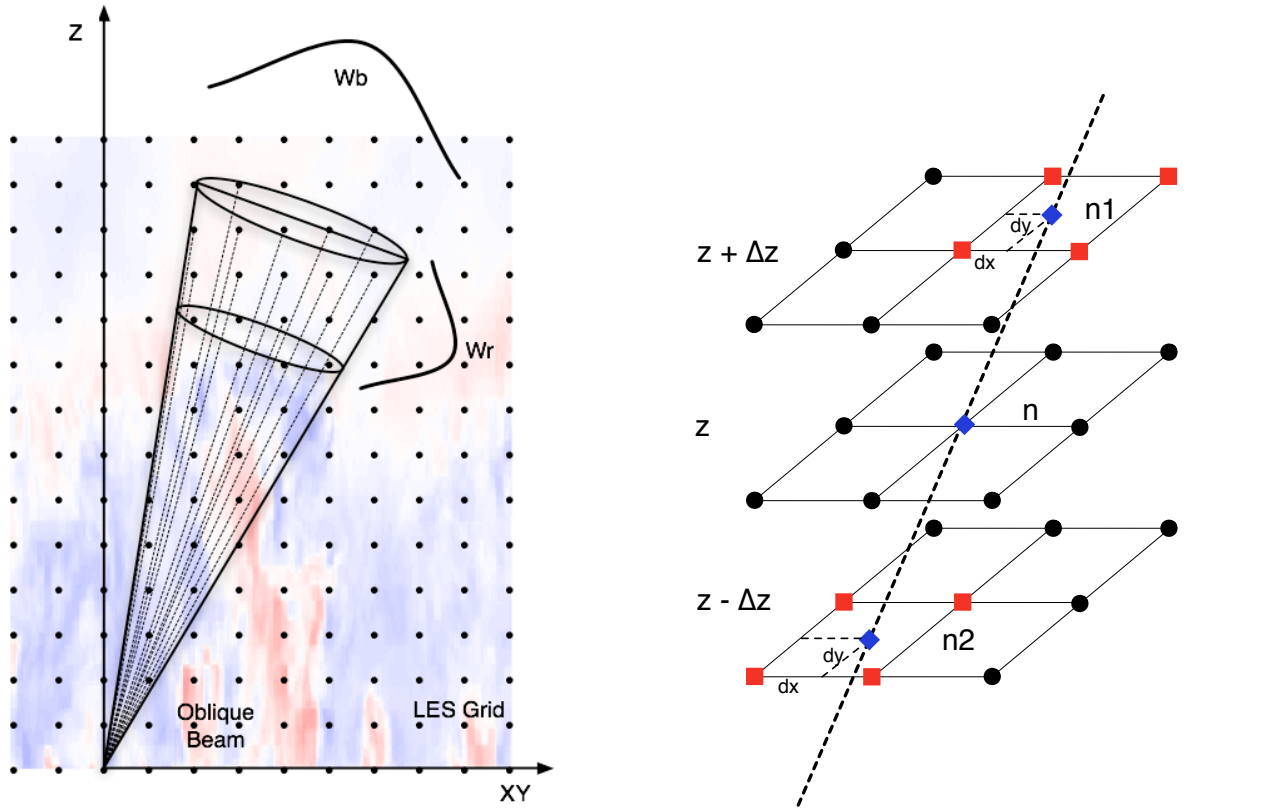

Figure 2: Left: scheme that represents an off-vertical pointing beam. The dotted lines represent the distance from the location of the radar to the grid points of the LES within the resolution volume. Along these dotted lines, C_n^2 is calculated, and later weighted in range (W_r) and beam width (W_b). Right: the dotted line represents the axis along which C_n^2 needs to be estimated. First the value of n at level z is obtained from the LES matrix, however at levels $z + \Delta z$ and $z - \Delta z$ the dotted line does not match any of the LES grid points. In order to obtain an estimate at those heights, a linear interpolation is made using the four closest points. Finally an average of the two gradients of n (from z and $z + \Delta z$, and z and $z - \Delta z$) is computed.

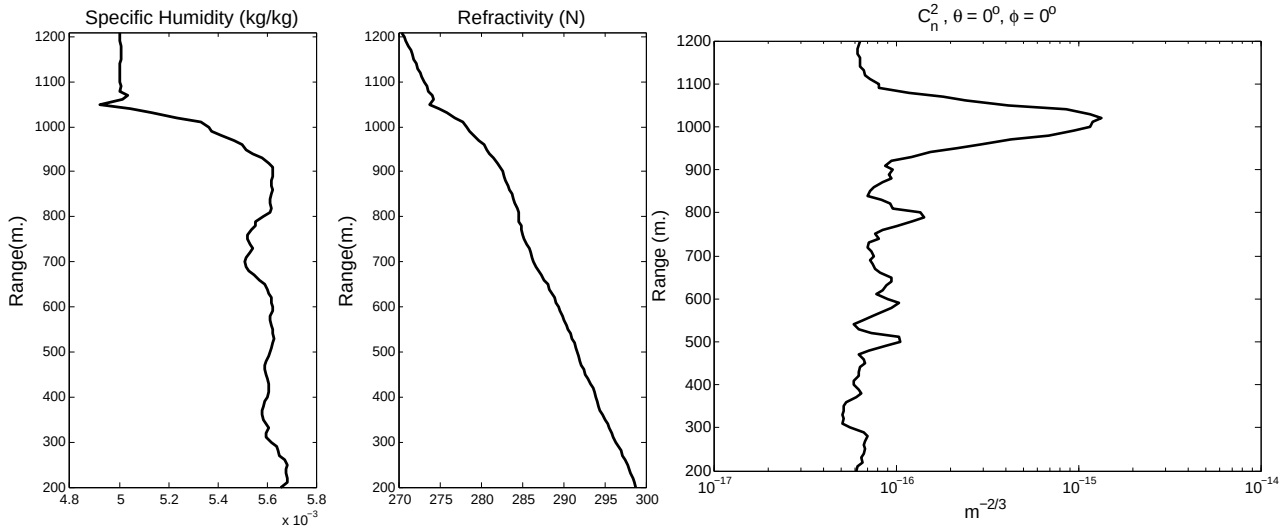

Figure 3: Left: vertical profile of specific humidity characteristic for the CBL. Center: vertical profile of the refractivity calculated from the LES fields. Right: vertical profile of the horizontally-averaged structure function parameter of refractivity, C_n^2. All data were calculated from a single realization in time.

tor according to

$$V(t_0+\tau) = A' \sum_{p=1}^{N} \sqrt{C_n^2(t_0+\tau)^{(p)} W_r^{(p)} W_b^{(p)}} \cdot \exp[-j(\varphi_0^{(p)} + k_B \cdot r^{(p)} + \mathbf{k}_B^{(p)} \cdot \mathbf{v}^{(p)}(t_0+\tau)\tau)], \quad (9)$$

$$A' = \frac{G}{\lambda r_0^2} \sqrt{0.0330} k_B^{-11/6},$$

where p represents each individual grid point of the N points contained within the resolution volume, G is a constant proportional to the power transmitted and gain of the transmitter and receiver, $\varphi_0^{(p)}$ is a random initial phase, k_B is the Bragg wavenumber ($k_B = \frac{4\pi}{\lambda}$), $\mathbf{k}_B^{(p)}$ is the Bragg wave vector that is directed from the center of the antenna to the center of the p^{th} LES grid cell and has the magnitude of k_B, $r^{(p)}$ is the distance from the center of the antenna to the center of the cell, $\mathbf{v}^{(p)}$ is the instantaneous radial velocity. W_r represents the range weighting function and is described by Holdsworth and Reid [1995] as

$$W_r = \exp\left[\frac{(r-r_0)^2}{2\sigma_r^2}\right], \quad (10)$$

where r represents the projection of the range of each grid point ($\sqrt{x^2+y^2+z^2}$) over the pointing direction, r_0 is the range of the center of the scattered volume, and the variance $\sigma_r = 0.35 c\tau_p/2$, where c is the speed of light and τ_p is the pulse width [Doviak and Zrnić, 1993]. Finally, the beam-pattern weighting function (W_b) is defined by the following equation [Yu, 2000; Cheong et al., 2004]:

$$W_b = \exp\left[-\frac{(\theta_x - \overline{\theta_x})^2}{2\sigma_x^2} - \frac{(\theta_y - \overline{\theta_y})^2}{2\sigma_y^2}\right], \quad (11)$$

$$\theta_x = \tan^{-1}\left(\frac{x}{z}\right), \quad \theta_y = \tan^{-1}\left(\frac{y}{z}\right),$$

where $\overline{\theta_x}$ and $\overline{\theta_x}$ describe the antenna beam pointing in degrees and $\sigma_x = \sigma_y = \theta_1/2.36$ are proportional to the beam width (θ_1) in degrees. Significant improvements over the work presented by Muschinski et al. [1999] are: the values of C_n^2, that are calculated over oblique beams along the radial, and velocity are now being interpolated at each time τ, the range weighting function (W_r) is now included as part of the simulator, and a range term ($k_B \cdot r^{(p)}$) which is important for further multiple frequencies applications is now incorporated in the phase term.

Since the LES generates data for variables at a time step of one second, and the radar inter-pulse period (IPP) is on the order of milliseconds, an estimation of any of the variables X at $t_0 + \tau$ is needed. In order to achieve this, the desired value is calculated using a linear interpolation scheme presented by Cheong et al. [2004]:

$$X(t_0+\tau) = (1-\tau)X(t_0) + \tau X(t_1), \quad (12)$$

where t_0 and t_1 are two consecutive time steps of the LES τ is the intermediate value taken from 0 to 1.

3.1. Radar Setup

The virtual radar in this study is patterned after a Vaisala UHF BLR (LAP3000) operating at a central frequency of 915 MHz, with a half-power beam width of 9°. It is possible to direct the radar beam vertically or, electronically steered 23° off vertical along 4 different azimuth angles: 0°, 90°, 180°, and 270°. In the present study, different off-vertical positions and range resolutions were chosen to validate the virtual BLR. The parameters chosen for the virtual BLR are presented in Table 2.

Table 2: Virtual BLR - Specifications

Quantity	Value
Frequency	915 MHz
Wavelength	32.8 m
Full half-power beam width	9°
Inter-Pulse Period	5 ms
Resolution	50 m
Beam inclination	variable

In order to produce realistic results from the virtual UHF BLR, it is necessary to introduce additive white noise to our generated time-series data. First, the maximum power of the signal is estimated from the time-series data; then, the variance of the background is computed based on a desired Signal-to-Noise Ratio (SNR). The complex white noise is generated based on the assumption that it has a Gaussian distribution described by the previously calculated variance. This procedure is independently applied to the real and imaginary components of the time-series data. The complex Gaussian noise is simply added to the original time-series data. An example of time-series data corresponding to a vertically pointing beam is presented in Fig. 4. The additive complex Gaussian noise shown was calculated for an SNR of 55 dB.

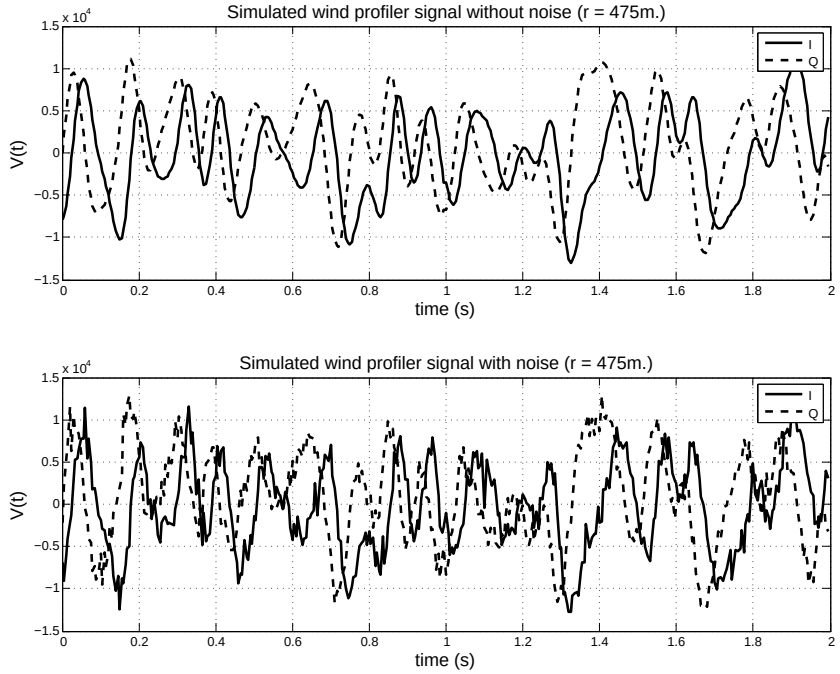

Figure 4: time-series data from the simulated BLR Data $V(t)$ obtained at a range of 475 m. The solid line represents the real part (in phase) of $V(t)$ and the dotted line is the imaginary part (quadrature) of $V(t)$. Top: without additive noise. Bottom: with additive Gaussian noise (SNR = 55 dB).

3.2. Spectral Analysis

A conventional spectral processing procedure was used to calculate the Doppler moments from the resulting complex time-series data (including the additive noise). First, the Doppler spectra were found, then the noise level was estimated using the algorithm described in Hildebrand and Sekhon [1974]. After the spectral levels were reduced to compensate for the estimated noise level, the first three moments were estimated (power, mean radial velocity, and spectrum width) following Doviak and Zrnić [1993].

An example of the spectral analysis is provided in Fig. 5 for a virtual radar located at x = 0 m, y = 0 m, and z = 0 m with respect to the center of the LES volume. The simulated radar beam has a width of 9° and is directed vertically. The range resolution was 50 m, and the profile shown was calculated with 2 coherent integrations and 20 sec of incoherent integration. Overall the results shown in each of the panels in Fig. 5 compare well with actual BLR data. Comparing the mean radial velocities estimated from the virtual BLR and the simulated "truth" from the LES (single profile pointing to the same direction), it can be seen that there is good agreement between the two datasets. Some differences are to be expected simply due to the disparate sizes of the sampling volumes resulting from a measurement along a single radial versus a 9° beam width. Although not shown here, additional radar simulator results were generated using a narrower beam width. Not surprisingly, the agreement between the estimated radial velocity and the simulated "truth" from the LES was improved, for this case.

We now consider the estimated signal power from the radar simulator. The center-right panel shows the range corrected power from the virtual BLR and the beam weighted C_n^2 ($W_b \cdot C_n^2$) obtained from the LES. The maximum of the range corrected power represents the top of the CBL, also known as the inversion layer, and its evolution over one hour of the simulation period can be observed in the bottom panel. Again, there exists a marked agreement between the simulated radar and LES fields.

4. STATISTICAL ANALYSIS

4.1. Experiment Setup

In order to perform a statistical analysis, a special experiment was designed. The so-called multiple radar exper-

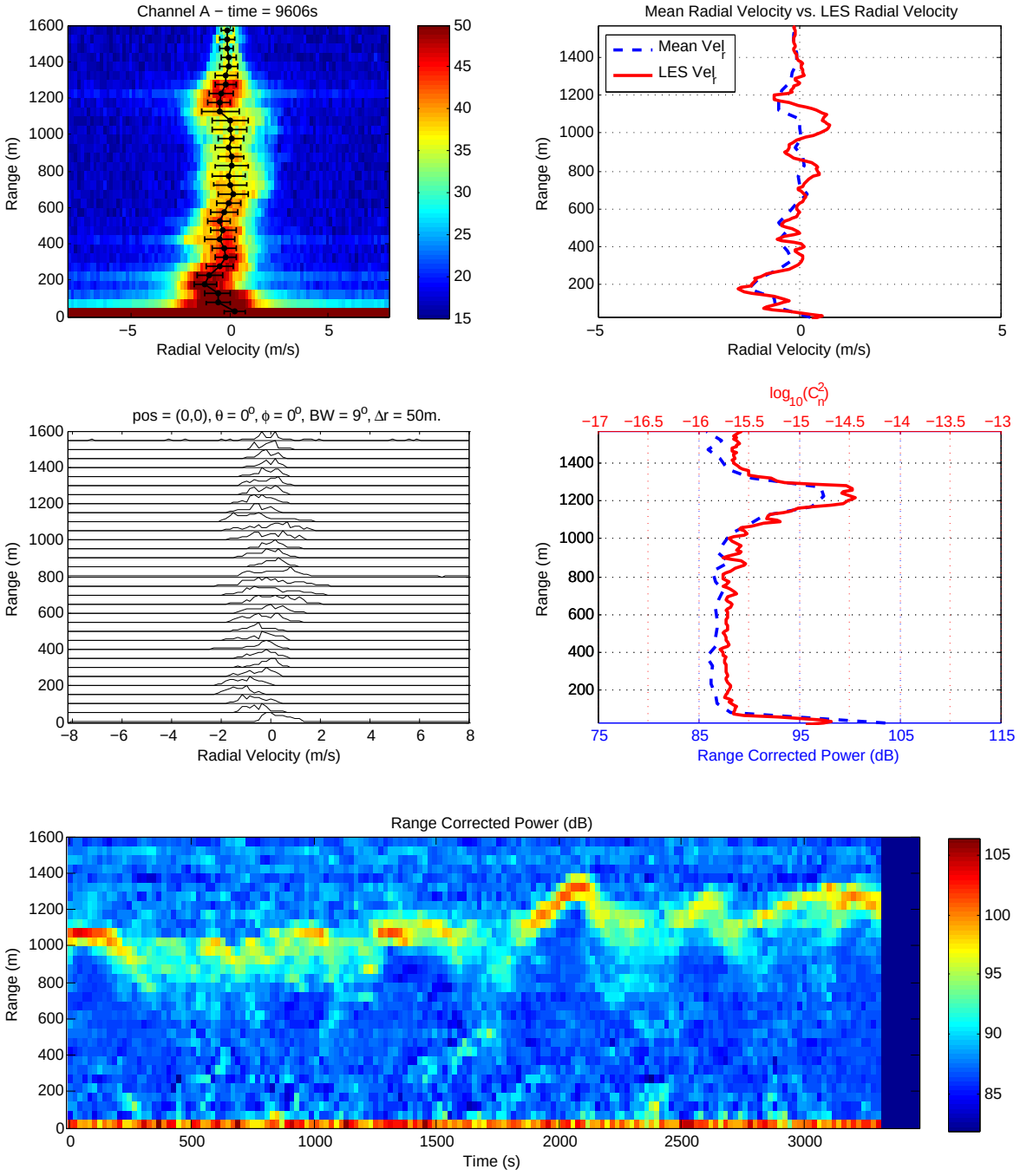

Figure 5: Spectral analysis of the time-series data at 9606 s. Top-left: intensity spectrum with additive white noise. The continuous line represents the mean radial velocity and the error bars the spectrum width. Top-right: comparison between the mean radial velocity estimated from the Doppler moments and the true radial velocity from the LES. Center-left: normalized stacked spectra. Center-right: comparison between the range corrected power estimated form the virtual radar and the beam weighted C_n^2 from the LES. The peak corresponds to the CBL top (inversion layer). Bottom: Range Corrected Power (dB) estimated form the LES for the whole simulation period.

iment (MRE) was designed using five different radars located equidistant from one another as illustrated in Fig. 6. The center radar within the LES domain used a vertically oriented beam. The other four radar beams were directed off-vertical (20°) but pointed towards the vertical beam of the first radar, at heights starting at 100 m up to 1500 m spaced every 100 m.

A procedure to validate the virtual radars is to compare the retrieved wind velocity vector from the virtual BLR to the "truth" from the LES. The mean radial velocity for the five radars was estimated following the procedure described in Section 3. The radial velocity is a function of the three dimensional wind field components u, v, w, the azimuth angle θ, and zenith angle ϕ as given by

$$v_r(\theta,\phi) = u\sin(\theta)\sin(\phi) + v\cos(\theta)\sin(\phi) + w\cos(\phi). \quad (13)$$

After combining the 5 radars with Doppler Beam Swinging (DBS) techniques the three-dimensional wind components can be retrieved. The obtained winds at each height can be directly compared with the ones from the LES as presented in Fig. 7, as can be observed, there is good agreement between estimates from the MRE and the "truth" from the LES.

4.2. Second-order Turbulence Statistics

The retrieved values from the MRE are used to estimate the turbulence kinetic energy (TKE), and the turbulent momentum fluxes over one hour of the simulation, these values are compared with data from the LES. The procedure involves estimating the deviations from the mean winds (u', v', and w'), which are used to estimate the variances and covariances used in the calculations. The variances from the LES are composed of two terms (Eq. 14). The first term represents the resolved variance obtained directly from the mean wind components, while the second term represents the subgrid component, which is calculated from the time-averaged subgrid kinetic energy (E_i). The total TKE (E_{TOTAL}) is obtained from the half-sum of the variances.

$$\sigma^2_{u_i}(LES) = \overline{u_i' u_i'} + \frac{2}{3}\overline{E_i}, \quad (14)$$

$$E_{TOTAL}(LES) = \frac{1}{2}\left(\sigma^2_u + \sigma^2_v + \sigma^2_w\right),$$

$$\sigma^2_{u_{ir}}(Radar) = \overline{u_{ir}' u_{ir}'}, \quad (15)$$

$$E_{TOTAL}(Radar) = \frac{1}{2}\left(\sigma^2_{ur} + \sigma^2_{vr} + \sigma^2_{wr}\right),$$

where u_i' and E_i are the i component of the velocity vector and subgrid kinetic energy respectively.

The obtained estimates of TKE are presented in Fig. 8. Both resolved and subgrid components of the TKE from the LES are shown. It can be observed that subgrid energy contributes to less than 10% of the variance in the LES case. The variances from the radar calculated over 100 m tend to underestimate the results from the LES (calculated over 10 m). The same behavior is observed in the total TKE.

As in the calculation of the turbulent kinetic energy, the vertical components of momentum flux from LES are composed of two terms (Eq. 16). The first term represents the co-variance obtained directly from the resolved wind components, while the second term represents the subgrid component.

$$K_{mi} = 0.12\Delta\sqrt{E_i},$$

$$\tau_{xz}(LES) = \overline{u'w'} + \overline{K_{mi}\frac{\partial u_i}{\partial z}},$$

$$\tau_{yz}(LES) = \overline{v'w'} + \overline{K_{mi}\frac{\partial v_i}{\partial z}}, \quad (16)$$

$$\tau_{xz}(Radar) = \overline{u_r' w_r'},$$

$$\tau_{yz}(Radar) = \overline{v_r' w_r'}, \quad (17)$$

where τ_{iz} represents the component of the vertical kinematic momentum flux; K_{mi} the subgrid-scale turbulent exchange coefficient; and $\Delta = \sqrt[3]{\Delta x \times \Delta y \times \Delta z}$ is the effective grid spacing, which in this case is 10 m.

In Fig. 9 the estimates of the vertical kinematic momentum flux components are presented. The components are presented in separate lines with their resolved and subgrid components, similar to TKE. As can be observed, the subgrid contribution represents less than 2% of the co-variance in the LES case. The flux components from the radar, even when calculated with 1/10 the LES resolution, generally follows the trend of the LES statistics.

5. CONCLUSIONS

Based on the work of Muschinski et al. [1999], an enhanced radar simulator has been presented for studies of the atmospheric convective boundary layer. This simulator is capable of producing realistic time-series data for idealized CBLs and has sufficient flexibility for a wide range of virtual radar experiments. For example, one can select the beam direction, beam width, pulse width, and simultaneously deploy a large number of virtual radars; as in the case of the MRE, which constitutes an inexpensive way to test various theories. Good agreement is observed from the wind retrieval obtained

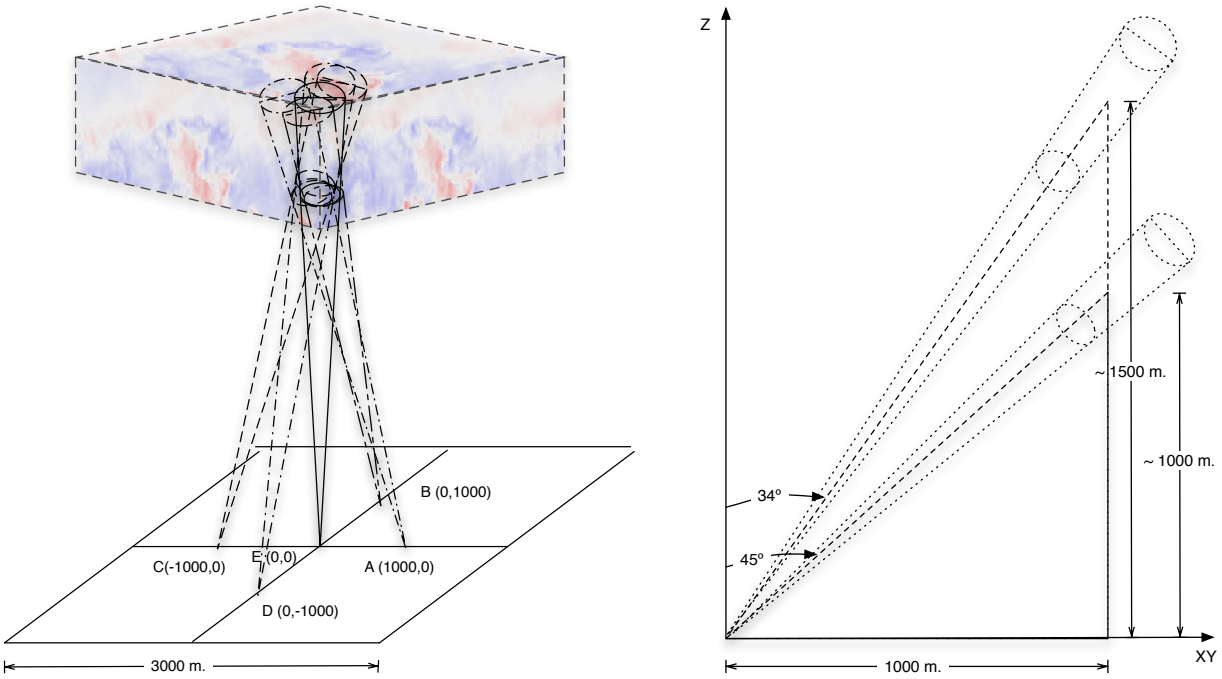

Figure 6: Multiple radar experiment Setup. The experiment was conducted using five radars pointing approximately towards the same resolution volume. Left: location of the radars (four oblique and one vertical pointing beams). Right: geometry of the radars pointing at only two different heights (∼1000 m and ∼1500 m), the idea is to have equidistant spacing (100 m) starting at 100 m up to 1500 m, which will cover almost all the LES vertical sub-domain.

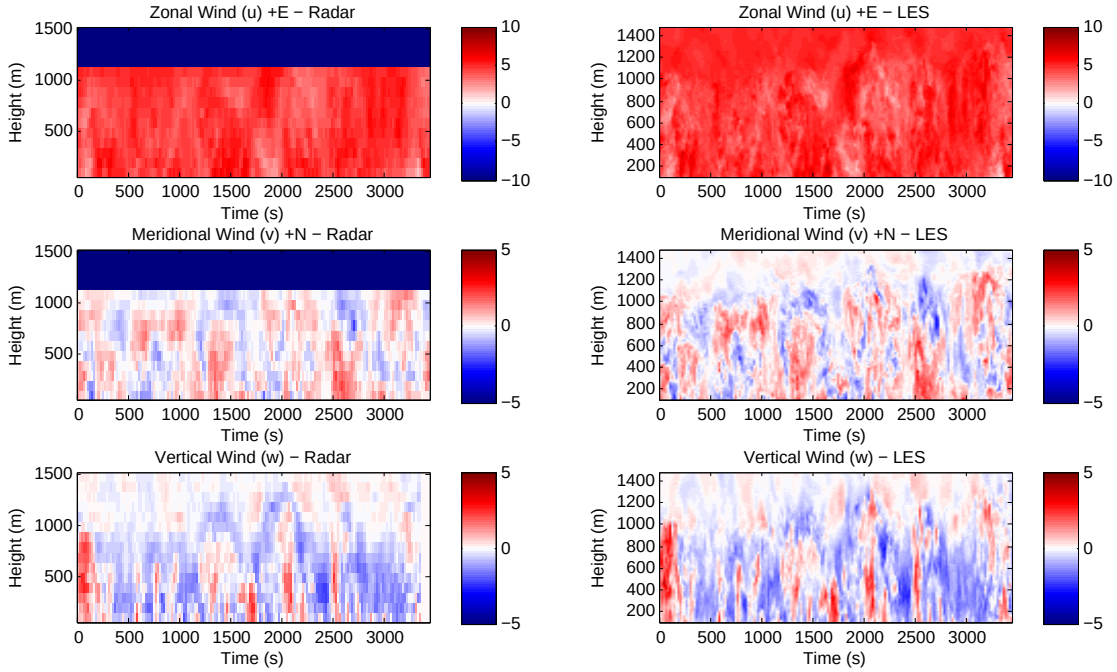

Figure 7: Comparison of the three-dimensional velocity field retrieved from the multiple radar arrangement using DBS (left) to the field obtained from LES at the center of the subdomain (right).

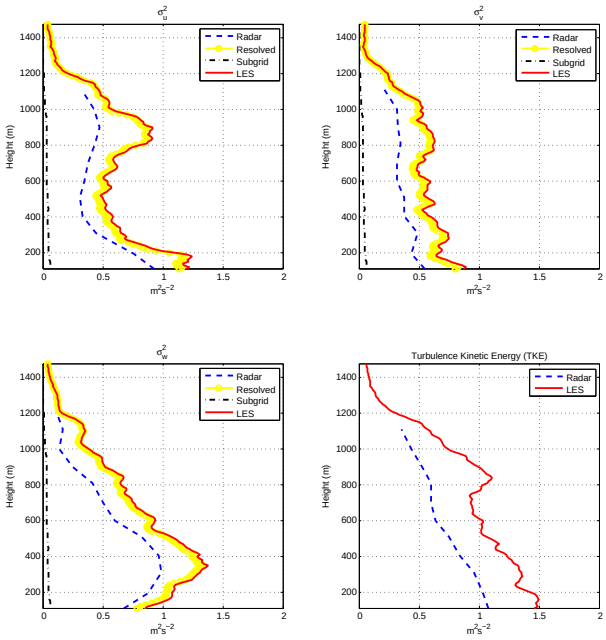

Figure 8: Variances of the velocity components and total estimates of TKE. The variances from the LES are being decomposed in resolved and subgrid components. Even though the radar estimates are calculated at about 1/10 the LES resolution, they follow the tendencies of the LES statistics.

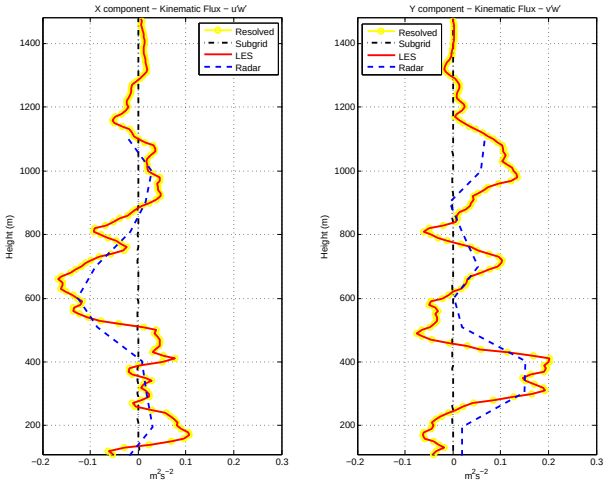

Figure 9: Vertical kinematic momentum flux components (X and Y). The LES fluxes are decomposed in resolved and subgrid parts. Again the subgrid component is very small, and the radar estimates fairly trail the ones from the LES.

from DBS from the 5 radars at each height with the point measurements of the LES. This agreement is also observed in the estimates of the TKE and the vertical components of the kinematic momentum fluxes.

ACKNOWLEDGMENTS

Support for this work was provided by the National Science Foundation under Grant No. 0553345.

References

Angevine, W. M., 1999: Entraintment results with advection and case studies from Flatland boundary layer experiments. *J. Geophys. Res.*, **104**, 30947–30963.

Angevine, W. M., A. B. White, and S. K. Avery, 1994: Boundary-layer depth and entrainment zone characterization with a boundary-layer profiler. *Boundary-Layer Meteor.*, **68**, 375–385.

Balsley, B. B., and K. Gage, 1982: On the use of radars for operational profiling. *Bull. Amer. Meteor. Soc.*, **63**, 1009–1018.

Bean, B. R., and E. J. Dutton, 1966: *Radio Meteorology*. Vol. 92 of *Natl. Bur. Stand. Monogr.* Supt. Doc. U.S. Govt. Printing Office, Washington D.C.

Cheong, B. L., M. W. Hoffman, and R. D. Palmer, 2004: Efficient atmospheric simulation for high-resolution radar imaging application. *J. Atmos. Oceanic Technol.*, **21**, 374–378.

Cohn, S. A., and W. M. Angevine, 2000: Boundary level height and entrainment zone thickness measured by lidars and wind-profiling radars. *J. Appl. Meteorol.*, **39**, 1233–1247.

Conzemius, R. J., and E. Fedorovich, 2006: Dynamics of sheared convective boundary layer entrainment. Part I: Meteorological background and large-eddy simulations. *J. Atmos. Sci.*, **63**, 1151–1178.

Dabberdt, W. F., G. L. Frederick, R. M. Hardesty, W. C. Lee, and K. Underwood, 2004: Advances in meteorological instrumentation for air quality and emergency response. *Meteor. Atm. Phys.*, **87**, 57–88.

Doviak, R. J., and D. S. Zrnić, 1993: *Doppler Radar and Weather Observations*. Academic Press, San Diego, CA, second edition.

Ecklund, W. L., K. S. Gage, and C. R. Williams, 1995: Tropical precipitation studies using a 915-MHz wind profiler. *Radio Sci.*, **30**, 1055–1064.

Fedorovich, E., R. Conzemius, I. Esau, F. K. Chow, D. Lewellen, C.-H. Moeng, D. Pino, P. Sullivan, and J. V.-G. de Arellano, 2004: Entrainment into sheared convective boundary layers as predicted by different large eddy simulation codes. in *Preprints, 16th Symp. on Boundary Layers and Turbulence, Amer. Meteor. Soc., 9-13 August, Portland, Maine, USA*, pp. CD–ROM, P4.7.

Fedorovich, E., F. T. M. Nieuwstadt, and R. Kaiser, 2001: Numerical and laboratory study of horizontally evolving convective boundary layer. Part I: Transition regimes and development of the mixed layer. *J. Atmos. Sci.*, **58**, 70–86.

Gage, K. S., C. R. Williams, and W. L. Ecklund, 1994: UHF wind profilers: A new tool for diagnosing and classifying tropical cloud systems. *Bull. Amer. Meteor. Soc.*, **75**, 2289–2294.

Grimsdell, A. W., and W. M. Angevine, 2002: Observation of the afternoon transition of the convective boundary layer. *J. Appl. Meteorol.*, **41**, 3–11.

Hildebrand, P. H., and R. S. Sekhon, 1974: Objective determination of the noise level in doppler spectra. *J. Appl. Meteorol.*, **13**, 808–811.

Holdsworth, D. A., and I. M. Reid, 1995: A simple model of atmospheric radar backscatter: Description and application to the full correlation analysis of spaced antenna data. *Radio Sci.*, **30**, 1263–1280.

Holton, J. R., 2004: *An Introduction to Dynamic Meteorology*. Elsevier Academic Press, fourth edition.

Holtslag, A. A. M., and P. G. Duynkerke, 1998: Clear and cloudy boundary layers. in *Royal Netherlands Academy of Arts and Sciences, Amsterdam*, p. 372.

Muschinski, A. P., P. P. Sullivan, R. J. Hill, S. A. Cohn, D. H. Lenschow, and R. J. Doviak, 1999: First synthesis of wind-profiler signal on the basis of large-eddy simulation data. *Radio Sci.*, **34**, 1437–1459.

Nieuwstadt, F. T. M., 1990: Direct and large-eddy simulation of free convection. in *Proc. 9th Internat. Heat Transfer Conference*, pp. 37–47.

Ottersten, H., 1969: Mean vertical gradient of potential refractive index in turbulent mixing and radar detection of CAT. *Radio Sci.*, **4**(12), 1247–1249.

Rogers, R. R., W. L. Ecklund, D. A. Carter, K. S. Gage, and S. A. Ethier, 1993: Research applications of a boundary-layer wind profiler. *Bull. Amer. Meteor. Soc.*, **74(4)**, 567–580.

Sheppard, E. L., and M. F. Larsen, 1992: Analysis of model simulations of spaced antenna/radar interferometer measurements. *Radio Sci.*, **27**, 759–768.

Tatarskii, V. I., 1961: *Wave Propagation in a Turbulent Medium*. McGraw-Hill, New York.

Wilczak, J. M., E. E. Gossard, W. D. Neff, and W. L. Eberhard, 1996: Ground-based remote sensing of the atmospheric boundary layer: 25 years of progress. *Boundary-Layer Meteor.*, **78**, 321–349.

Yu, T.-Y., 2000: *Radar studies of the atmosphere using spatial and frequency diversity*. Ph.D. thesis, University of Nebraska, Lincoln, Nebraska.

Zilitinkevich, S. S., 1991: Turbulent penetrative convection. in *Avebury Technical, Aldershot*, p. 179.